JACS
JOURNAL OF THE AMERICAN CHEMICAL SOCIETY
Article
Cite This: J. Am. Chem. Soc. 2019, 141, 20249−20260
pubs.acs.org/JACS

Diuranium(IV) Carbide Cluster U_2C_2 Stabilized Inside Fullerene Cages

Jiaxin Zhuang,[†,⊥] Laura Abella,[§,⊥] Dumitru-Claudiu Sergentu,[§,⊥] Yang-Rong Yao,[∥] Meihe Jin,[†] Wei Yang,[†] Xingxing Zhang,[†] Xiaomeng Li,[†] Duo Zhang,[‡] Yiming Zhao,[†] Xiaohong Li,[†] Shuao Wang,[‡] Luis Echegoyen,[∥] Jochen Autschbach,[*,§] and Ning Chen[*,†]

[†]Laboratory of Advanced Optoelectronic Materials, College of Chemistry, Chemical Engineering and Materials Science, and [‡]School of Radiological and Interdisciplinary Sciences & Collaborative Innovation Center of Radiation Medicine of Jiangsu, Higher Education Institutions, Soochow University, Suzhou, Jiangsu 215123, People's Republic of China

[§]Department of Chemistry, University at Buffalo, State University of New York, Buffalo, New York 14260, United States

[∥]Department of Chemistry, University of Texas at El Paso, 500 West University Avenue, El Paso, Texas 79968, United States

Supporting Information

ABSTRACT: Novel actinide cluster fullerenes, $U_2C_2@I_h(7)$-C_{80} and $U_2C_2@D_{3h}(5)$-C_{78}, were synthesized and fully characterized by mass spectrometry, single-crystal X-ray crystallography, UV−vis−NIR, nuclear magnetic resonance spectroscopy (NMR), X-ray absorption spectroscopy (XAS), Raman spectroscopy, IR spectroscopy, as well as density functional and multireference wave function calculations. The encapsulated U_2C_2 is the first example of a uranium carbide cluster featuring two U centers bridged by a C≡C unit. The U−C bond distances in these U_2C_2 clusters are in the range between 2.130 and 2.421 Å. While the U_2C_2 cluster in $U_2C_2@C_{80}$ adopts a butterfly-shaped geometry with a U−C_2−U dihedral angle of 112.7° and a U−U distance of 3.855 Å, the U−U distance in $U_2C_2@C_{78}$ is 4.164 Å and the resulting U−C_2−U dihedral angle is increased to 149.1°. The combined experimental and quantum-chemical results suggest that the formal U oxidation state is +4 in the U_2C_2 cluster, and each U center transfers three electrons to the C_{2n} cage and one electron to C_2. Different from the strong U=C covalent bonding reported for $U_2C@C_{80}$, the U−C bonds in U_2C_2 are less covalent and predominantly ionic. The C−C triple bond is somewhat weaker than in HCCH, and the C−C π bonds undergo donation bonding with the U centers. This work demonstrates that the combination of the unique encapsulation effect of fullerene cages and the variable oxidation states of actinide elements can lead to the stabilization of novel actinide clusters, which are not accessible by conventional synthetic methods.

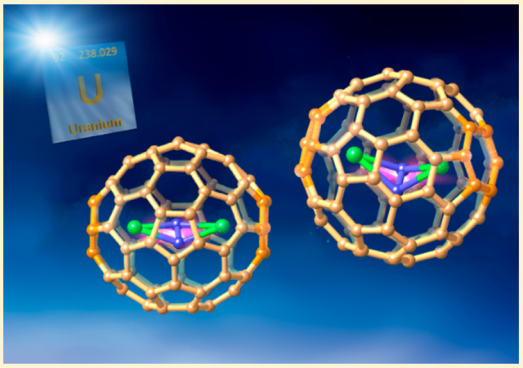

1. INTRODUCTION

Actinide endohedral metallofullerenes (EMFs) are novel fullerenes that encapsulate actinide atoms and clusters. The exploration of encapsulated actinides inside fullerene cages dates back to 1992 when Smalley et al. reported mass spectra of a series of uranium-based EMFs.[1] Although some effort was devoted to the encapsulation of other actinides inside fullerene cages in subsequent years,[2−5] it took until 2017 for the first full characterization of an actinide EMF, $Th@C_{3v}(8)$-C_{82}.[6] Our recent success in the synthesis and characterization of actinide metallofullerenes shows that their physiochemical properties and electronic structures are not only substantially different from those of the conventional EMFs based on lanthanides, but also different from other actinide compounds.[7−12] For instance, some of the known monometallic actinide EMFs represent the first examples of tetravalent metals encapsulated inside fullerene cages.[6,10,12] The unique four-electron metal-to-cage charge transfer and the resulting unusually strong metal−cage interactions lead to the stabilization of some unexpected non-isolated-pentagon-rule cages, which otherwise are not stable either in their empty form or with encapsulation of lanthanide atoms.[10] Moreover, actinides were found to adopt variable oxidation states depending on the cage structures or clusters, which is notably very different from the common Ln^{3+} oxidation state in the lanthanide based EMFs.[7−9,13−15]

Recently, we reported the first actinide cluster fullerene $U_2C@I_h(7)$-C_{80}.[9] The encapsulated uranium carbide cluster, U=C=U, was unprecedented as it possessed two unsupported U=C bonds, never before observed in other molecular structures. Inside the fullerene cage, this diuranium carbide cluster adopted an unintuitive nonlinear U=C=U configuration. Quantum-chemical calculations showed that both U atoms have a formal +5 oxidation state. This study

Received: September 23, 2019
Published: December 3, 2019

DOI: 10.1021/jacs.9b10247
J. Am. Chem. Soc. 2019, 141, 20249−20260

demonstrated that it is feasible to observe novel endohedral structures with new actinide clusters and bonding motifs. Known uranium carbides exist in the form of uranium monocarbide (UC), diuranium tricarbide (U_2C_3), and uranium dicarbide (UC_2), and these act as refractory ceramic materials and fuel for nuclear reactors.[16−20] Such fuel is intended for nuclear-powered rockets due to its better power density, and uranium carbides are desirable candidates for new generations of nuclear reactors at very high temperatures.[16,19] In this context, understanding the electronic structures and physical and chemical properties of uranium carbides has significant importance.

Herein, we report the synthesis of two novel uranium carbide cluster EMFs, $U_2C_2@I_h(7)$-C_{80} and $U_2C_2@D_{3h}(5)$-C_{78}, both of which were characterized by mass spectrometry, single-crystal X-ray crystallography, nuclear magnetic resonance spectroscopy (NMR), X-ray absorption spectroscopy (XAS), UV−vis−NIR, Raman spectroscopy, IR spectroscopy, as well as density functional theory (DFT) and multireference wave function calculations. The experimental and theoretical studies confirm that U takes a different oxidation state in the novel encapsulated uranium clusters, U^{4+}, than in the previously reported $U_2C@I_h(7)$-C_{80} (U^{5+}). $U_2C_2@I_h(7)$-C_{80} and $U_2C_2@D_{3h}(5)$-C_{78} are the first examples of structurally characterized uranium(IV) carbides (U_2C_2 motif), forming a butterfly shape in which the two bridged C atoms are linked by a C≡C triple bond. In particular, $U_2C_2@I_h(7)$-C_{80} represents the first example of hexavalent M_2C_2 cluster that can be embedded in an $I_h(7)$-C_{80} fullerene cage. The computational studies also reveal that, while U_2C inside $I_h(7)$-C_{80} contains two covalent U−C double bonds, the U−C bonds in the $U_2C_2@I_h(7)$-C_{80} and $U_2C_2@D_{3h}(5)$-C_{78} are predominantly ionic with some covalent character, indicating that uranium clusters are able to display remarkably different electronic properties and bonding inside fullerene cages.

2. RESULTS AND DISCUSSION

2.1. Synthesis and Isolation of $U_2C_2@C_{2n}$ ($2n$ = 78, 80). Carbon soot containing uranium-based endohedral fullerenes was produced by a modified Krätschmer−Huffman arc discharge method. Graphite rods, packed with U_3O_8 and graphite powder (molar ratio of U/C = 1:30), were vaporized in the arcing chamber under a 200 Torr He atmosphere. The resulting soot was then collected and extracted with CS_2 for 12 h. Multistage HPLC procedures were employed to isolate and purify $U_2C_2@C_{2n}$ ($2n$ = 78, 80) (Figures S1 and S2). The purity of the isolated $U_2C_2@C_{2n}$ ($2n$ = 78, 80) was confirmed by the observation of single peaks by HPLC. The positive-ion mode MALDI-TOF mass spectra of purified $U_2C_2@C_{80}$ and $U_2C_2@C_{78}$ show peaks at 1460.041 and 1436.021 m/z (Figure 1), respectively. In addition, the experimental isotopic distributions of the two samples both agree well with theoretical predictions.

2.2. Molecular and Electronic Structures of $U_2C_2@I_h(7)$-C_{80}·[Ni^{II}-OEP] and $U_2C_2@D_{3h}(5)$-C_{78}·[Ni^{II}-OEP]. The molecular structures of $U_2C_2@C_{80}$ and $U_2C_2@C_{78}$ were unambiguously determined by single-crystal X-ray diffraction analyses. To get single crystals of fullerenes with resolvable data could be quite challenging due to super severe disorder caused by the rotation of fullerenes. The presence of the cocrystallized agent can improve the crystallinity of fullerenes and effectively hinder the rotation of fullerenes. This technique developed by the Balch and Olmstead group and the most

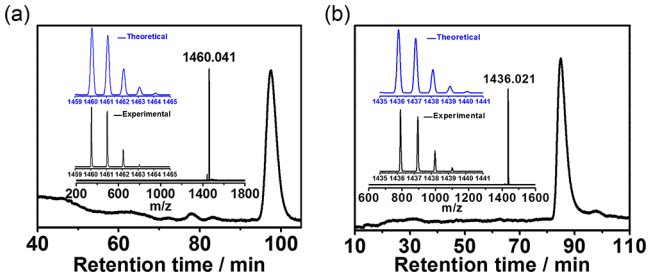

Figure 1. HPLC chromatogram of purified $U_2C_2@C_{80}$ on a Buckyprep column (a) and $U_2C_2@C_{78}$ on a 5PBB column (b) with toluene as the eluent. HPLC condition, λ = 310 nm; flow rate, 4 mL/min. The insets show the positive-ion mode MALDI-TOF mass spectra and expansions of the corresponding experimental isotopic distributions of $U_2C_2@C_{80}$ and $U_2C_2@C_{78}$ in comparison with the theoretical ones.

commonly used ones are metal porphyrin compounds such as Ni-, Co-, or Cu-octaethylporphyrin.[21−23] Here, we use Ni^{II}-octaethylporphyrin (Ni^{II}-OEP, OEP = 2, 3, 7, 8, 12, 13, 17, 18-octaethylporphyrin dianion) as cocrystallized agent. Slow diffusion of this compound in benzene into the CS_2 solution of the corresponding EMFs yielded black block crystals. The structures were solved and refined in the $P2_1/c$ (No. 14) space group. Figures 2a and 4a show the molecular structures of

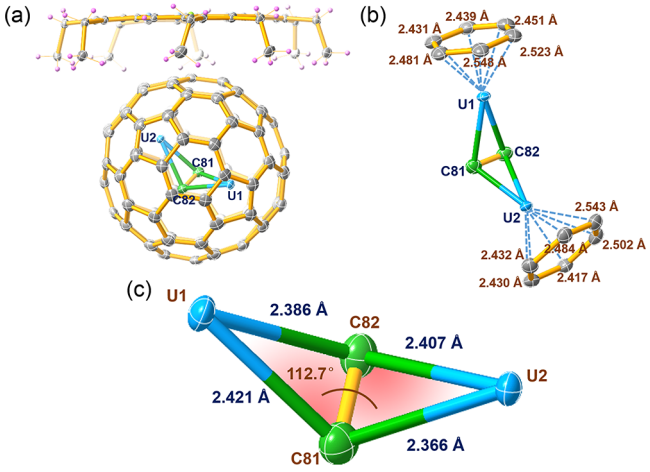

Figure 2. (a) ORTEP drawing of $U_2C_2@I_h(7)$-C_{80}·[Ni^{II}(OEP)] with 20% thermal ellipsoids. Only the major U sites (U1 and U2 with occupancies of 0.849(5) and 0.630(7)) are shown. For clarity, the solvent molecules and minor metal sites are omitted. (b) View showing the relationship of the major U_2C_2 cluster with the closest cage portions. (c) Configuration of the endohedral U1−C_2−U2 fragment.

these two compounds together with the cocrystallized Ni^{II}-(OEP) molecules. The shortest contacts between the Ni and a cage carbon for $U_2C_2@I_h(7)$-C_{80}·[Ni^{II}-OEP] (Ni1−C64) and $U_2C_2@D_{3h}(5)$-C_{78}·[Ni^{II}-OEP] (Ni1−C62B) are 2.770 and 2.814 Å, respectively, suggesting $\pi-\pi$ interactions between the fullerene cages and the Ni^{II}(OEP).

Molecular and Electronic Structures of $U_2C_2@I_h(7)$-C_{80}. The crystallographic data of $U_2C_2@I_h(7)$-C_{80}·[Ni^{II}-OEP] indicate that the $I_h(7)$-C_{80} cage along with the internal carbon atoms C81 and C82 are fully ordered. Although the U atoms are somewhat disordered, two major U positions (U1 and U2) have particularly high occupancies of 0.849(5) and 0.630(7),

DOI: 10.1021/jacs.9b10247
J. Am. Chem. Soc. 2019, 141, 20249−20260

Table 1. Experimentally Geometric Parameters of U_2C_2 Unit in $U_2C_2@I_h(7)$-C_{80} and Interatomic Parameters of Carbide Clusters in Selected Fullerenes[a]

	$U_2C_2@I_h(7)$-C_{80}	$Sc_2C_2@D_{3h}(14246)$-C_{74}	$Sc_2C_2@C_{2v}(5)$-C_{80}	$Sc_2C_2@C_{3v}(8)$-C_{82}	$Sc_2C_2@D_{2d}(23)$-C_{84}
C−C/Å	1.233(11)	1.05	1.197(7)/1.196(9)	1.19(1)−1.20(2)	1.20(1)
M−M/Å	3.855	3.888(16)−4.474(9)	4.312(3)	3.86(1)−4.09(3)	4.435(5)−4.47(2)
dihedral angle/deg	112.7	120.8	127.0(3)−130.8(3)	127.9(6)−145(1)	149.4(8)−154.3(7)

[a]Values taken from refs 21 and 26.

Table 2. Experimentally Derived Geometric Parameters of U_2C_2 Unit in $U_2C_2@I_h(7)$-C_{80} and $U_2C_2@D_{3h}(5)$-C_{78} in Comparison with the U_2C Unit in $U_2C@I_h(7)$-C_{80}[a]

		$U_2C_2@D_{3h}(5)$-C_{78}		
	$U_2C_2@I_h(7)$-C_{80}	major	minor	$U_2C@I_h(7)$-C_{80}
C−C/Å	1.233(11)	1.127(18)	1.11(2)	
M−M/Å	3.855	4.164	4.174	3.849
M−C/Å	2.421(8)/2.386(9)/ 2.366(8)/2.407(8)	2.130(13)/2.23(3)/ 2.354(12)/2.21(3)	2.073(13)/2.26(4)/ 2.390(12)/2.26(5)	2.033(5)/2.028(5)
dihedral angle/deg	112.7	149.1	146.6	142.8
ring centroid distance/Å	7.86	8.01	8.03	7.93

[a]Values taken from ref 9.

respectively. As a result, the U_2C_2 cluster inside the $I_h(7)$-C_{80} cage can be considered almost fixed with the occupancies of residual U sites ranging from 0.0127(11) to 0.221(5) (Table S1).

It is noteworthy that $U_2C_2@I_h(7)$-C_{80} represents the first example for a M_2C_2 cluster stabilized inside an $I_h(7)$-C_{80} cage, which is well-known for its stabilization by a 6-electron transfer. Thus, the crystallographic structure of this compound indicates that, different from the typical 4 electron transfer observed between encapsulated M_2C_2 and C_{2n} fullerene cages, here, the U_2C_2 likely transfers 6 electrons to the $I_h(7)$-C_{80} cage.

The major U1 and U2 sites both reside at the center of hexagons, and the distances between U1, U2 sites and the carbons of the corresponding aromatic rings of the cage all lie within the range of 2.417(8)−2.548(8) Å (Figure 2b and Table S2). A closer analysis of the U_2C_2 cluster reveals that the C−C length is 1.233(11) Å, which is comparable with those reported for typical fullerene carbides, that is, $Sc_2C_2@C_{2v}(5)$-C_{80} (1.197(7)/1.196(9) Å),[24] $Sc_2C_2@C_{3v}(8)$-C_{82} (1.19(1)−1.20(2) Å),[24] $Sc_2C_2@D_{2d}(23)$-C_{84} (1.20(1) Å),[24] $Tm_2C_2@C_s(6)$-C_{82} (1.28 Å),[25] $Tb_2C_2@C_s(6)$-C_{82} (1.232(2) Å),[26] $Sc_2C_2@C_{2v}(9)$-C_{86} (1.212(4) Å),[27] and $Sc_2C_2@C_s(hept)$-C_{88} (1.215(7) Å).[28] Apparently, similar to most encapsulated metallic carbides based on lanthanides, the U_2C_2 cluster adopts a butterfly-shaped geometry with a U−C_2−U dihedral angle of 112.7° and a U−U distance of 3.855 Å, as shown in Figure 2c. The U−U distance is similar to that observed in the U_2C cluster in $U_2C@I_h(7)$-C_{80} (3.849 Å).[9] As compared to encapsulated lanthanide carbides, which exhibit a similar butterfly arrangement, the bent U_2C_2 cluster inside $I_h(7)$-C_{80} cage is notably more compressed, with a smaller dihedral angle and a shorter metal−metal distance, as summarized in Table 1.[24,29]

The U−C bond lengths vary over a narrow range of 2.366(8)−2.421(8) Å (Figure 2c and Table 2), which are significantly longer than the U−C distance (2.033(5)/2.028(5) Å) in the previously reported $U_2C@C_{80}$. In $U_2C@C_{80}$, the two U−C bonds were determined to be axial double bonds.[9] Thus, U−C distances in U_2C_2 seem to be closer to the distance of U−C single bond. On the other hand, in conventional actinide compounds, molecular structures with two U bridged by two N,[30] O,[31] H,[31] S,[32] or Cl[33] have been reported before. However, actinide compounds containing U_2C_2 motif, that is, two U bridged by two C, has never been reported so far, neither in the solid nor in the gas phase. The closest reported bonding motif of the U−C single bond might be uranium metallocene complexes, reported by Evans et al.[34] Here, the experimentally observed U−C bond lengths of $U_2C_2@I_h(7)$-C_{80} are comparable to those for U(IV)−C single bond metallocene complexes: 2.425(2) Å for $(C_5Me_4SiMe_3)_2UMe_2$, 2.453(2) Å for $(\eta5{:}\eta1$-$C_5Me_4SiMe_2CH_2)_2U$, as well as 2.385(2) and 2.397(2) Å for $(\eta5{:}\eta2$-$C_5Me_4SiMe_2CH_2C{=}N^tBu)_2U$.[34] However, the U−C distances of $U_2C_2@I_h(7)$-C_{80} are still significantly shorter than those found in other representative uranium(IV) complexes (2.476(13)−2.660(7) Å), indicating a more folded structure of the U_2C_2 cluster and stronger interaction between uranium atoms and the carbons inside the cage.[33,35−37]

Theoretical calculations were employed to further understand the unique electronic structure and bonding nature for $U_2C_2@I_h(7)$-C_{80}. Starting with the X-ray coordinates, the structure was optimized for various spin states using Kohn−Sham DFT with nonhybrid ("pure") and hybrid functionals. The calculated relative adiabatic spin-state energies and structural parameters are reported in Tables S6−S8.

The hybrid functionals agree on a spin-quintet ground state (GS) for $U_2C_2@I_h(7)$-C_{80} and produce excellent agreement with the experimental X-ray structure. Within the $I_h(7)$-C_{80} cage, the U_2C_2 fragment adopts a butterfly shape and tends to remain in a position where the U atoms are located close to the centers of carbon hexagons, in agreement with the low disorder positions of the crystallographic data (Figure S8 and Table S9). Figure 3 summarizes the calculated data for the $U_2C_2@I_h(7)$-C_{80} GS. The calculated C−C distance of the U_2C_2 fragment is 1.26 Å, 0.03 Å longer than the one measured. The C−C distance suggests a weaker C−C bond order than in the triple C−C bond of acetylene (1.20 Å), but a similar overall bond order as in the alleged quadruple bond of C_2 (1.24 Å). As shown below, U_2C_2 features a weakened C−C triple bond. In the spin-quintet GS, the electronic structure is

DOI: 10.1021/jacs.9b10247
J. Am. Chem. Soc. 2019, 141, 20249−20260

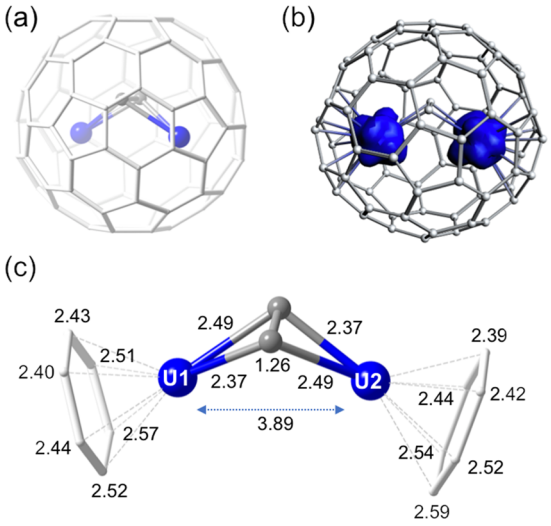

Figure 3. (a) Optimized GS structure of $U_2C_2@I_h(7)$-C_{80} (ZORA/PBE0/TZP/D3). (b) ±0.01 isosurfaces of the spin density. (c) Equilibrium distances, in angstrom, for the encapsulated U_2C_2 fragment and adjacent carbons.

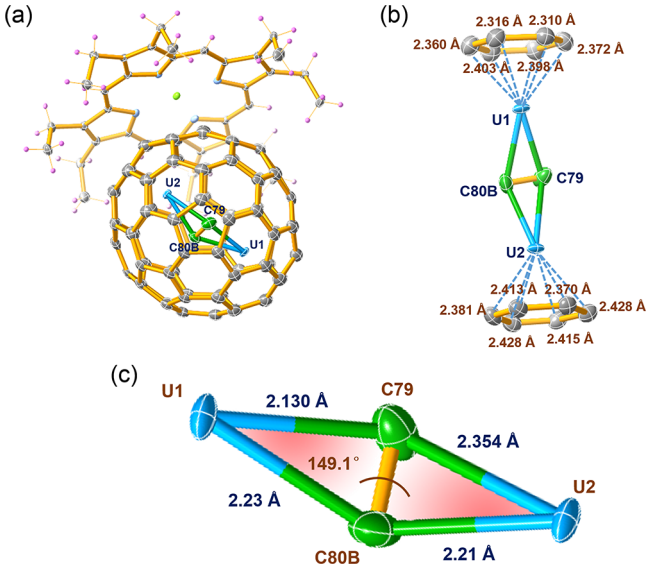

Figure 4. (a) ORTEP drawing of $U_2C_2@D_{3h}(5)$-C_{78}·[Ni^{II}(OEP)] with 20% thermal ellipsoids. Only the major U_2C_2 site (U1 and U2 with occupancies of 0.427(3) and 0.425(4)) and cage A (0.425(4) occupancy) are shown. For clarity, the solvent molecules and minor metal sites are omitted. (b) View showing the relationship of the major U_2C_2 cluster with the closest cage portions in the major cage. (c) Configuration of the endohedral U1−C_2−U2 fragment.

consistent with $(U_2C_2)^{6+}@(C_{80})^{6-}$: Each U center transfers three electrons to the $I_h(7)$-C_{80} host cage and one electron to the bridged C_2 moiety, attaining a formal oxidation state of +4. This aspect is confirmed (i) by the Mulliken spin populations showing that there are two unpaired electrons per U center (Table S6), and (ii) by the spin density also showing that the unpaired density is localized at the metal centers (Figure 3b).

Molecular and Electronic Structures of $U_2C_2@D_{3h}(5)$-C_{78}. $U_2C_2@D_{3h}(5)$-C_{78} shows fullerene cage disorder over two orientations with occupancies of 0.575(4) (cage B) and 0.425(4) (cage A). Although there are 14 U sites in the cage, only four major sites will be discussed here, and they can be paired into two sets according to their similar occupancies, the U1/U2 pair (occupancy 0.427(3)/0.425(4)) and the U3/U4 pair (occupancy 0.367(3)/0.3654(19)). The other minor sites are summarized in Table S3. The internal carbon atom C79 is fully ordered, while C80 has two disordered sites, C80A and C80B, with the occupancies of 0.37(4) and 0.63(4), respectively. On the basis of crystallographic and structural logic, the major U_2C_2 unit (U1−C79−C80B−U2) should be assigned to cage A (occupancy 0.425(4)) and the minor U_2C_2 unit (U3−C79−C80A−U4) to cage B (occupancy 0.575(4)). For clarity, only the major U_2C_2 site and cage A are shown in Figure 4a. As shown in Figure 4b, U1 and U2 both reside close to the center of two symmetric hexagons with U-cage distances in the range of 2.310−2.428 Å, and the positions of U3 and U4 are similar to those of U1 and U2 with the shortest U-cage distances ranging from 2.331 to 2.442 Å (Figure S5a). The inner C−C bond lengths for the major (C79−C80B) and minor clusters (C79−C80A) are 1.127(18) and 1.11(2) Å, respectively, which are slightly shorter than that in $U_2C_2@C_{80}$ (1.233(11) Å). The following analyses will only focus on the U_2C_2 cluster with major occupancies (U1−C79−C80B−U2) in C_{78} because of the geometric similarities between these two sites, and more details are provided in Table 2 and Figure S5b. For the carbide moiety, the U−C bond lengths fall in the range 2.130(13)−2.354(12) Å, which are evidently shorter than those of uranium carbene complexes[32,33,36,37] and a set of complexes that possess a double dative bond between carbon and uranium in the latest study by Zhu and co-workers.[38] It is noteworthy that these U−C bond lengths are even shorter than those in $U_2C_2@C_{80}$. On the other hand, despite similar butterfly-shaped geometries, the shape of the U_2C_2 cluster in C_{78} is considerably more stretched than that in C_{80}. Such varying structural features can be ascribed to the different cage shapes of C_{80} and C_{78}. For $D_{3h}(5)$-C_{78}, the cage is more oval, so the U_2C_2 can be better accommodated. Specifically, the longest distances of the ring centroid of the corresponding hexagons in C_{80} and C_{78} are 7.86 and 8.01 Å, respectively. Notably, the U−U distance in $U_2C_2@C_{78}$ is 4.164 Å, significantly longer than 3.855 Å observed in $U_2C_2@C_{80}$, and the resulting U−C_2−U dihedral angle is 149.1°. Except for a few examples ($Sc_2C_2@D_{2d}(23)$-C_{84},[24] $La_2C_2@C_s(574)$-C_{102}, and $La_2C_2@C_2(816)$-C_{104}[39−41]), the U−C_2−U dihedral angles are notably larger than for most of the characterized butterfly-shaped carbide-containing EMFs.[24,26,41,42]

Starting from the X-ray coordinates, the molecular structure of $U_2C_2@D_{3h}(5)$-C_{78} was optimized for various spin multiplicities with DFT. Adiabatic spin-state relative energies and structural parameters are reported in Tables S10−S12. Both pure and hybrid functionals agree on a spin-triplet GS for $U_2C_2@D_{3h}(5)$-C_{78}, although a spin-quintet is predicted by the hybrid functionals to be close in energy, within ∼5 kcal mol^{-1} of the triplet. The spin-triplet and spin-quintet equilibrium geometries obtained with PBE0 are shown in Figures S9 and 5, respectively. The spin-quintet structure reproduces more closely the U_2C_2 fragment geometry from the X-ray study. The calculated Raman spectrum (vide infra) for the quintet also agrees much better with the experimental spectrum. Therefore, we tentatively conclude that the DFT calculations have difficulties in predicting the correct spin state ordering for this system and proceed with the spin-quintet. As for $U_2C_2@I_h(7)$-C_{80}, the $U_2C_2@D_{3h}(5)$-C_{78} cluster fullerene affords a $(U_2C_2)^{6+}@(C_{78})^{6-}$ charge distribution and U^{4+} metal centers, as confirmed (i) by the Mulliken spin populations (∼2 per U

DOI: 10.1021/jacs.9b10247
J. Am. Chem. Soc. 2019, 141, 20249−20260

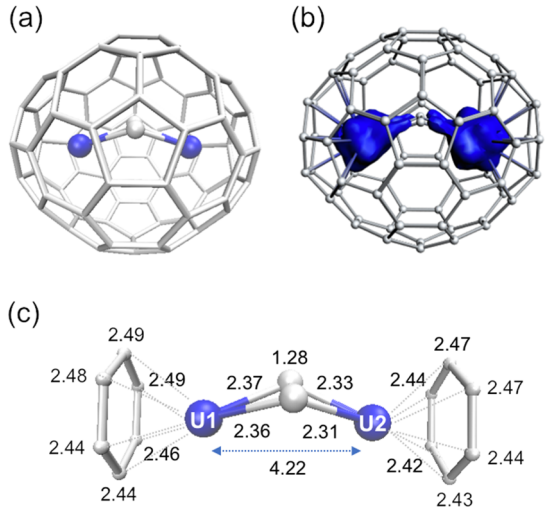

Figure 5. (a) Optimized geometry for the lowest energy spin-quintet state of U_2C_2@$D_{3h}(5)$-C_{78} (ZORA/PBE0/TZP/D3). (b) ±0.01 isosurfaces of the spin density. (c) Equilibrium distances, in angstroms, for the encapsulated U_2C_2 fragment and adjacent carbons.

center, Table S10) and (ii) by the spin density (Figure 5b), showing that the unpaired density is localized at the metal centers.

In the $D_{3h}(5)$-C_{78} cage, the U_2C_2 unit adopts a butterfly arrangement in which the U atoms tend to remain in positions close to the centers of carbon hexagons (Figures 5a, S10, and S11, and Tables S13 and S14), just as in the $I_h(7)$-C_{80} cage. Optimized cluster fullerene geometries with U_2C_2 orientations perpendicular to the optimal orientation shown in Figure 5a show compressed U1−C_X−U2 (X = 1, 2) bond angles, very short U1−U2 distances, and very high energies (e.g., orientations 3 and 4 in Figure S10, and orientation 4 in Figure S11). Therefore, the $D_{3h}(5)$-C_{78} cage favors a U_2C_2 unit with wider U1−C_X−U2 (X = 1, 2) bond angles than does the $I_h(7)$-C_{80} cage.

2.3. Computational Study of Molecular Structure and Bonding in a Model System $UC_2U@(C_7H_7)_2$ (1). To obtain information on the relation between the U_2C_2 substructure and the host cage (C_{80} vs C_{78}), we sought to characterize the geometry and bonding of a model structure, $UC_2U@(C_7H_7)_2$ (**1**), displaying no cage steric hindrance but faithfully reproducing the charge and spin distribution of U_2C_2 in the parent cluster fullerenes.

In the model complex **1**, each of the two U centers attains the formal +4 oxidation state by transferring three electrons to the coordinating C_7H_7 unit and one electron to the C_2 unit. The electronic structure therefore is consistent with a formal $[U]^{4+}[C_2]^{2-}[U]^{4+}@[(C_7H_7)_2]^{6-}$ charge distribution, and the system adopts a ground spin-quintet state with four electrons localized at the U^{4+} centers, as in the parent cluster fullerenes. Starting from a geometry, which replicates well the optimized $U_2C_2@C_6$ fragment of $U_2C_2@I_h(7)$-C_{80} (see structure **1a** of Figure S12), optimization of **1** using C_{2v} symmetry led to a nearly planar U_2C_2 fragment (Figure S12, structure **1c**), with U1−C_2−U2 dihedral angles wider by 59.6° and 23.2° than the observed dihedral angles within C_{80} and C_{78}, respectively. The U−C (2.53 Å) and C_2 (1.27 Å) distances are also longer than the measured values (2.40 Å on average for U−C and 1.23 Å for C_2 within C_{80}, 2.23 Å on average for U−C and 1.23 Å for C_2 within C_{78}). Optimization of **1** starting from structure **1a** but constraining the cycloheptatrienyl ligand coordinates resulted in U−C (2.52 Å) and C_2 (1.26 Å) distances that are only 0.01 Å shorter than in the aforementioned fully optimized structure of **1** (see structure **1b** of Figure S12). Once again, the increasing tendency of the U1−C_2−U2 dihedral angle from 111.4° to 118.7° is noted. Hence, the opening of the U1−C_2−U2 dihedral angle in the fully optimized geometry **1c** or constrained geometry **1b** is not a consequence of the chemical bonding within the U_2C_2 fragment. The dihedral angle increase happens in the absence of the steric hindrance of the fullerene cages. For instance, the C_2 distance is found to be similar in **1** (1.26 or 1.27 Å depending on the geometry considered) and in the optimized full cluster (1.26 Å), and only 0.01 Å shorter than for a PBE0/TZ2P/D3BJ optimized C_2^{2-} free ion (1.28 Å), suggesting predominantly ionic U−C_2 interactions.

NLMO/DFT bonding analyses, performed for the optimized model geometries **1b**, **1c**, as well as the full systems $U_2C_2@C_{2n}$ ($2n$ = 78, 80), determine overall similar chemical bonding within the U_2C_2 fragment (Figures 6 and S13). In particular, there are three two-electron NLMOs, one σ and two π, describing the triple bond of C_2^{2-}. All of them have some four-center character due to a delocalization toward the neighboring U centers. The σ NLMO has ∼96% total weight from C 2s−2p hybrids and ∼4% weight from U based 6d−5f hybrids. The four-center character is larger for the π NLMOs, which have contributions between 12% and 16% from the two U centers. The visual inspection of the NLMO isosurfaces in Figure 6 allows for a qualitative distinction between the carbon and U interactions. The σ NLMO appears to be polarized toward the U centers mainly as a result of electrostatic interactions, while the π NLMOs are sufficiently strongly delocalized onto the U centers to assign a degree of donation bonding between the C_2^{2-} fragment and the metal centers. Weak donation bonding from C_2^{2-} to U occurs also through the C-2s lone pairs, as these delocalize toward the metal atoms to form two three-center U1−C−U2 bonds with weight contributions from the U centers between 14% and 18%. Density depletion from the C_2^{2-} unit toward the neighboring U atoms, by itself, cannot justify the shortening of the C_2^{2-} length by 0.01 Å from the isolated free anion to within the encapsulated U_2C_2 fragment. The observed shorter C_2 bond

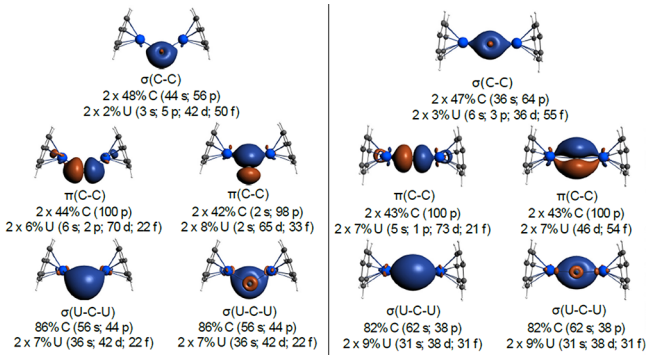

Figure 6. NLMO isosurfaces (±0.03 au) and atomic orbital % compositions obtained from a natural bond orbital analysis of the ZORA/DFT/PBE0 quintet state obtained for the optimized structures **1b** (left panel) and **1c** (right panel) (see Figure S12) of the model complex **1**.

DOI: 10.1021/jacs.9b10247
J. Am. Chem. Soc. 2019, 141, 20249−20260

length within $U_2C_2@I_h(7)$-C_{80} must be a result of a delicate balance between U1−C_2−U2 bonding and steric hindrance.

To support the conclusions derived from the DFT calculations, complete active space (CAS) self-consistent field (SCF) wave function-based calculations were performed for **1**. Structure **1a** (Figure S12) was retained in these calculations as (i) it models best the U_2C_2−C_{80} interaction in $U_2C_2@I_h(7)$-C_{80}, and (ii) it affords the same electronic structure and bonding of U_2C_2 as in $U_2C_2@I_h(7)$-C_{80}. As for the parent cluster fullerenes, the GS of **1** can be expected to exhibit multiconfigurational character and to be accompanied by a manifold of low-lying excited states, due to the (near-) degeneracy of the U-5f levels, aspects that are known to be problematic for DFT with available approximate functionals. CAS(4, 10) calculations predicted four orbitally (nearly) degenerate spin-quintet states describing the GS. Calculated electronic states and GS (a $^5A_2$) natural orbitals are shown in Table S15 and Figure S14, respectively. Triplet and singlet excited states occur at high energies, 1.05 ($^3B_2$) and 2.22 ($^1A_1$) eV above the GS, and are therefore not strongly involved in spin−orbit coupling (SOC) with the GS quintets. Indeed, a state-interaction calculation involving all possible spin-quintet states afforded by the active space together with 50 spin-triplet and 50 spin-singlet states per irreducible representation concluded with a spin−orbit GS of essentially spin-quintet character. NLMO analyses of the CAS(4, 10) and CAS(4, 10)+SOC ground-state wave functions, provided in Figure S15, both agreed on a bonding picture for the U_2C_2 fragment that is nearly identical with the DFT/NLMO analyses for the optimized structures of **1** (Figure 6) and for the optimized structures of the cluster fullerenes (Figure S13). The fact that the U_2C_2 chemical bonding obtained with multiconfigurational approaches is unchanged from the chemical bonding obtained with DFT is in part due to the fact that the unpaired electrons occupy U-based 5f orbitals of mostly nonbonding character.

2.4. Spectroscopic Studies. The UV−vis−NIR absorption spectra of the two compounds are shown in Figure 7. The absorption spectrum of $U_2C_2@I_h(7)$-C_{80} is rather featureless in that only one minor peak at 683 nm is observed, which is very similar to typical $I_h(7)$-C_{80} cage-based fullerenes.[8,9] The absorption spectrum of $U_2C_2@D_{3h}(5)$-C_{78} displays one pronounced peak at 584 nm and a broad peak at 776 nm. These absorption features bear no resemblance to those of reported lanthanide cluster fullerenes of $Sc_3N@D_{3h}$-C_{78}[43] and $Ti_2S@D_{3h}$-C_{78},[44] although they share the same D_{3h}-C_{78} cage symmetry and electronic structure. It appears that the embedded actinide cluster has a major impact on the absorption behavior of actinide endohedral fullerenes. Thus, unlike what has been commonly accepted in the study of lanthanide-based EMFs, these results show that the UV−vis−NIR spectra of actinide endohedral fullerenes cannot be taken as the fingerprint proof for the determination of the cage symmetry or electronic structure of EMFs. The purified sample of $U_2C_2@I_h(7)$-C_{80} has a yellow brown color, and $U_2C_2@D_{3h}(5)$-C_{78} presents a gray brown color in CS_2.

Nuclear magnetic resonance (NMR) spectroscopy was used to characterize $U_2C_2@I_h(7)$-C_{80} as shown in Figure 8. The ^{13}C NMR spectrum of $U_2C_2@I_h(7)$-C_{80} measured at 298 K shows two signals at 132.23 and 106.42 ppm with a ca. 3:1 intensity ratio, corresponding to the sets of 60 and 20 equivalent carbon atoms of the $I_h(7)$-C_{80} fullerene cage.[9,45−47] The ^{13}C NMR spectrum measured at a higher temperature of 308 K shows slightly shifted signals at 132.78 and 107.42 ppm, respectively, with a slightly smaller chemical shift difference ($\Delta\delta$ = 25.36 ppm) than that observed at 298 K ($\Delta\delta$ = 25.81 ppm). Such a trend is very similar to what we have observed for $U_2C@I_h(7)$-C_{80}[9] and previously reported $Ce_2@I_h(7)$-C_{80},[47] in which a paramagnetic effect of encaged cluster on the chemical shift of ^{13}C signal was observed. On the other hand, the temperature dependence of $\Delta\delta/\Delta T$ = 0.045 ppm/K is relatively weak, similar to that of $U_2C@I_h(7)$-C_{80} ($\Delta\delta/\Delta T$ = 0.02 ppm/K). The NMR data are consistent with the paramagnetic nature of the electronic ground-state manifold of the U_2C_2 fragment, and furthermore indicate that the open uranium 5f shells are only weakly involved in covalent bonding with the fullerene cage. If it were otherwise, the ^{13}C signals from the fullerene would likely show a stronger temperature dependence, due to contact

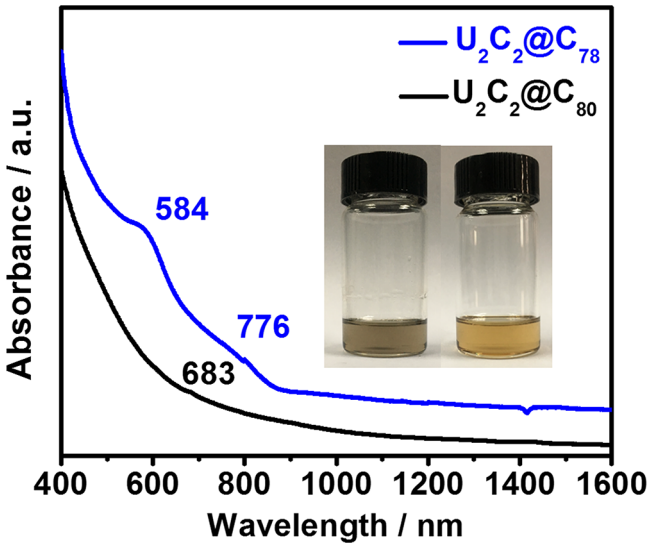

Figure 7. UV−vis−NIR spectra of $U_2C_2@I_h(7)$-C_{80} (black) and $U_2C_2@D_{3h}(5)$-C_{78} (blue) in CS_2. The insets show the photographs of 0.3 mg of $U_2C_2@D_{3h}(5)$-C_{78} (left) and 0.3 mg of $U_2C_2@I_h(7)$-C_{80}(right) dissolved in 3 mL of CS_2 solution, respectively.

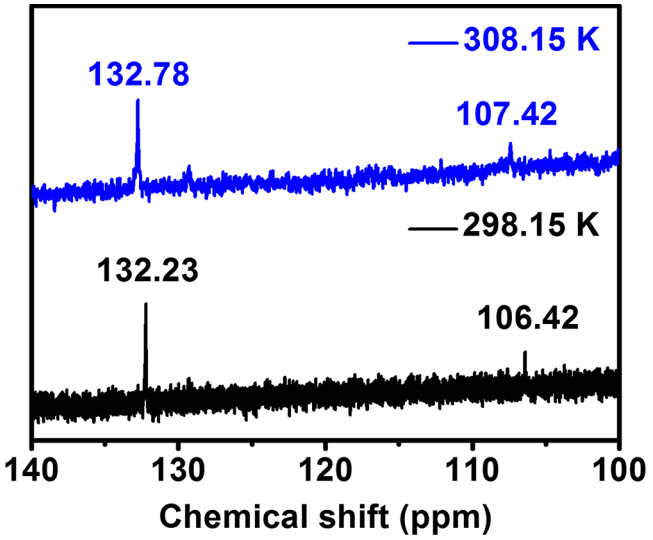

Figure 8. ^{13}C NMR (600 MHz) spectra of $U_2C_2@I_h(7)$-C_{80} (CS_2, 298 and 308 K). A capillary tube containing acetone-d_6 was used as an internal lock.

DOI: 10.1021/jacs.9b10247
J. Am. Chem. Soc. 2019, 141, 20249−20260

shifts. It is noteworthy that no signal was detected for the inner bridged C_2 carbon atoms, most likely due to the limited sample amount, as well as the fact that the two carbons could be strongly paramagnetically shifted and broadened.

The experimental and computational Raman and IR spectra of $U_2C_2@I_h(7)$-C_{80} and $U_2C_2@D_{3h}(5)$-C_{78} are shown in Figures S6 and S7. The major peaks of the Raman spectrum of $U_2C_2@I_h(7)$-C_{80} observed in the 200−500 cm^{-1} range are assigned to cage vibrational modes, which are typical for $I_h(7)$-C_{80} (Figure S6a).[8,9] The corresponding metal-to-cage vibration peak appears at 123 cm^{-1}, which is similar to those observed for U-based fullerenes.[8] As for $U_2C_2@D_{3h}(5)$-C_{78}, the first major peak at 148 cm^{-1} of the observed spectrum is the corresponding metal-to-cage vibration peak. The observed peaks between the range of 200−250 and 400−600 cm^{-1} are assigned to the cage vibrational mode (Figure S7b). The IR spectra of the two cluster fullerenes also show characteristic vibration peaks known for $I_h(7)$-C_{80} and $D_{3h}(5)$-C_{78} cages. The computational spectra agree well with the measured ones (Figures S17−S19).

The X-ray absorption spectroscopy (XAS) spectra for $U_2C_2@I_h(7)$-C_{80} and $U_2C_2@D_{3h}(5)$-C_{78} along with the reference compounds provide further experimental evidence for the identification of the oxidation state of U in $U_2C_2@C_{2n}$ ($2n$ = 78, 80). As shown in Figure 9, the white line peaks of

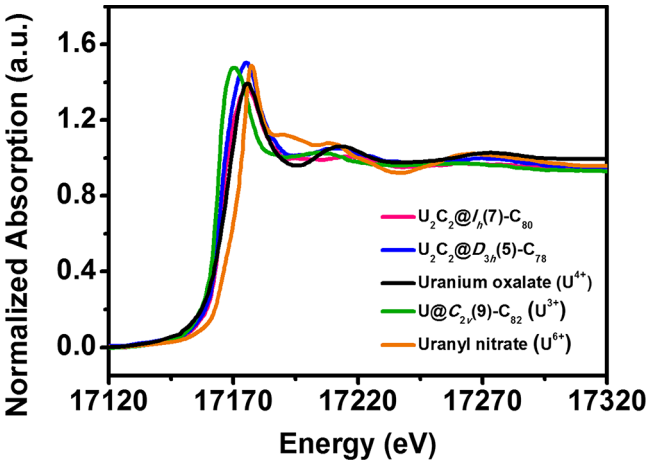

Figure 9. U L_3-edge XAS spectra of $U_2C_2@I_h(7)$-C_{80} and $U_2C_2@D_{3h}(5)$-C_{78}, as compared to those of $U@C_{2v}(9)$-C_{82} (U^{3+}), uranium oxalate (U^{4+}), and uranyl-nitrate (U^{6+}).

$U_2C_2@I_h(7)$-C_{80}, $U_2C_2@D_{3h}(5)$-C_{78}, and uranium oxalate (U^{4+}) are perfectly aligned, indicating the same oxidation state of +4. In addition, the energies of the white line peaks of $U_2C_2@I_h(7)$-C_{80} and $U_2C_2@D_{3h}(5)$-C_{78} are between those of the $U@C_{2v}(9)$-C_{82} (U^{3+}) and uranyl nitrate (U^{6+}). These results confirm that in $U_2C_2@I_h(7)$-C_{80} and $U_2C_2@D_{3h}(5)$-C_{78}, the U ions take +4 oxidation state, which is in agreement with the structural assignment and theoretical predictions.

2.5. Comparison of the Bonding in $U_2C_2@D_{3h}(5)$-C_{78} and $U_2C_2@I_h(7)$-C_{80}. Quantum-chemical calculations (vide supra) indicate that each metal atom has an $5f^2$ formal electronic configuration. In both cluster fullerenes and in the model compound **1**, the uranium centers transfer an aggregate of 6 electrons to the $I_h(7)$-C_{80}/$D_{3h}(5)$-C_{78} cages or C_7H_7 ligands; that is, the charge distributions agree with the $(U_2C_2)^{6+}@(C_{80})^{6-}$, $(U_2C_2)^{6+}@(C_{78})^{6-}$, and $(U_2C_2)^{6+}(C_7H_7)^{6-}$ configurations. Similar NLMOs are found for U_2C_2 within both C_{2n} cages and for the model complex, suggesting that the bonding of the U_2C_2 fragment does not depend strongly on the host cage, nor is it sensitive to changes in the geometrical parameters of U_2C_2 within the C_{2n} cages (see Figures 6, S13, and S15).

The U−C bonding in U_2C_2 is predominantly ionic, accompanied by some σ (less) and π (more) donation bonding from C_2^{2-} to the U 5f and 6d shells. These interactions are similar to those in Sc_2C_2 within C_{84} and C_{82} cages, or Y_2C_2 within C_{82}. The optimized structural parameters for the $U_2C_2@C_{2n}$ cluster fullerenes and model complex **1** suggest that all of these compounds feature a U_2C_2 unit with a bridged weak C−C triple bond (1.28 and 1.26 Å within $D_{3h}(5)$-C_{78} and $I_h(7)$-C_{80}, respectively, and 1.27 Å in **1**). Moreover, the U_2C_2 unit is flatter inside $D_{3h}(5)$-C_{78} than inside $I_h(7)$-C_{80}, but flat with the C_7H_7 ligands of the model complex **1**. The U_2C_2 flattening is dictated by the shape of the host cage: with a butterfly shape, a flatter U_2C_2 is accommodated within the $D_{3h}(5)$-C_{78} cage, as this cage has an oval shape with a longer inside dimension than that of the $I_h(7)$-C_{80} cage (8.129−8.240 Å, see Figure 10). In contrast, the height of the

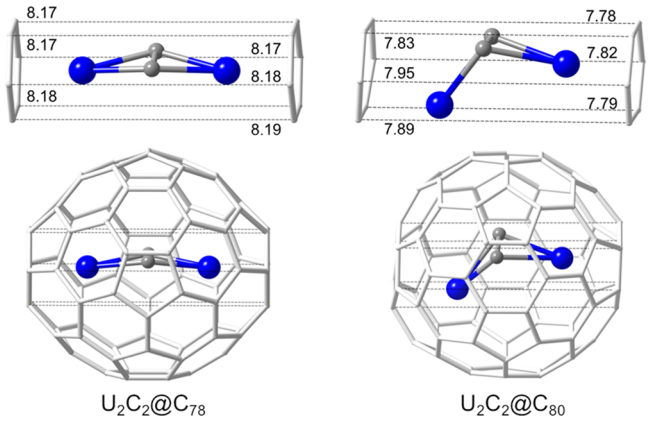

Figure 10. Comparison between the depth of $D_{3h}(5)$-C_{78} and $I_h(7)$-C_{80} cages. Model fragment is shown above the corresponding C_{2n} cage. Dashed lines indicate the depth of the C_{2n} cage. Distances are in angstrom.

$D_{3h}(5)$-C_{78} cage is 7.769 Å, that is, shorter than its maximum depth, resulting in the high energetics of the optimized $U_2C_2@D_{3h}(5)$-C_{78} geometries with U_2C_2 aligned with this direction. The depth of the $I_h(7)$-C_{80} cage is smaller (7.770−7.967 Å, Figure 10), which appears to cause the bending of U_2C_2. It is worth noting that the depth shrinkage from C_{78} to C_{80} is on average 0.32 Å, matching well with the U1−U2 distance shortening of 0.31 Å (experimentally) or 0.33 Å (computationally); see Tables S8 and S12 and Figures 3c and 5c, caused by the change in the U1−C_2−U2 dihedral angle. The U_2C_2 unit is nearly flat in the model complex **1**, due to the absence of cage steric hindrance; that is, the C_7H_7 ligands can move freely along with the U centers. Thus, the shape of the cage, with the steric hindrance it exerts, determines the nearly planar versus bent arrangement of the encapsulated U_2C_2 cluster.

2.6. Comparison of $U_2C_2@I_h(7)$-C_{80} and $U_2C@I_h(7)$-C_{80}. For the previously characterized $U_2C@I_h(7)$-C_{80} isomer, the bonding model showed strongly polarized double bond U=C interactions with partial π-overlap, strengthened by electrostatic attractive forces between cationic U^{5+} atoms and the anionic C^{4-} carbide bridge. In contrast, for $U_2C_2@I_h(7)$-C_{80},

DOI: 10.1021/jacs.9b10247
J. Am. Chem. Soc. 2019, 141, 20249−20260

the bonding in the UC_2U fragment is predominantly ionic, with comparatively weaker covalent character. It is interesting to compare the U_2C_2 moiety of $U_2C_2@I_h(7)$-C_{80} with the U_2C moiety of $U_2C@I_h(7)$-C_{80}. As shown herein, within the UC_2U fragment, the two uranium centers interact mainly through ionic with the carbon centers, and covalently, although weakly, with the bonding and nonbonding electron orbitals of the cylindrical C_2^{2-} fragment. While the UC_2U moiety shows a preference to be planar, it is easily distorted to fit within different fullerene cages. In comparison, the covalent interactions within the U_2C moiety of the previously reported $U_2C@I_h(7)$-C_{80} system are much more pronounced, and the fragment adopts a bent shape inside the fullerene as well as outside, with a U−C−U angle between 142.8° (experimental XRD) and 166° (calculations on $U_2C@I_h(7)$-C_{80} and on models where U_2C could potentially straighten out). As explained in the previous study of $U_2C@I_h(7)$-C_{80},[9] the bent structure of U_2C is related to the large electronegativity difference of C and U, which leads to bond polarization toward, and lone pair electron density build-up on, the carbon such that its optimal hybridization is between sp^1 and sp^2. Consequently, the angle between the σ bonding carbon hybrid AOs is between 120° and 180°.

3. CONCLUSIONS

In summary, unprecedented actinide cluster fullerenes, $U_2C_2@I_h(7)$-C_{80} and $U_2C_2@D_{3h}(5)$-C_{78}, have been successfully synthesized and characterized by mass spectrometry, single-crystal X-ray crystallography, UV−vis−NIR, nuclear magnetic resonance spectroscopy (NMR), X-ray absorption spectroscopy (XAS), Raman spectroscopy, IR spectroscopy, as well as DFT and multireference wave function calculations.

Crystallographic analyses unambiguously show that a novel uranium carbide cluster, U_2C_2, was encapsulated inside both $I_h(7)$-C_{80} and $D_{3h}(5)$-C_{78} cages. The U−C bond distances in these U_2C_2 cluster are in the range between 2.130 and 2.421 Å, indicative of U−C single bonds. The U_2C_2 cluster shows considerable structural flexibility inside the fullerene cages. While the U_2C_2 cluster in $U_2C_2@C_{80}$ adopts a butterfly-shaped geometry with a U−C_2−U dihedral angle of 112.7° and a U−U distance of 3.855 Å, the U−U distance in $U_2C_2@C_{78}$ is 4.164 Å and the U−C_2−U dihedral angle increases to 149.1°.

The combined experimental and quantum-chemical results suggest that the formal U oxidation state is +4 in the U_2C_2 cluster. Different from a typical 4-electron transfer from lanthanide-based Ln_2C_2 cluster to the carbon cage, U_2C_2 transfers 6 electrons to the fullerene cage, thus leading to the formation of the first $I_h(7)$-C_{80} cage stabilized M_2C_2 cluster.

For the previously characterized $U_2C@I_h(7)$-C_{80} isomer, the bonding model showed strongly polarized double bond U−C interactions with partial π-overlap, strengthened by electrostatic attractive forces between cationic U^{5+} atoms and the anionic C^{4-} carbide bridge. In contrast, for $U_2C_2@I_h(7)$-C_{80}, the bonding in the UC_2U fragment is predominantly ionic, with comparatively weaker covalent character.

While oxo- and nitro-bridged uranium motifs have been reported in previous studies, to the best of our knowledge, $U_2C_2@C_{2n}$ represents the first example in which a dicarbon bridged uranium bonding motif is stabilized. The C−C triple bond is somewhat weaker than the one in HCCH, and the C−C π bonds undergo donation bonding with the U centers. Computational results also suggest that, different from the inherently bent structure of U═C═U, the observed angle of the UC_2U "butterfly" structure is dependent on the steric hindrance imposed by the fullerene cage. In the absence of this hindrance, the U_2C_2 cluster prefers a planar structure.

This work demonstrates that, due to the variable oxidation states of actinide elements, the electronic structure and the bonding motif of endohedral actinide cluster fullerenes can be substantially different from those of their lanthanide analogues. Continuing efforts to synthesize and characterize these novel actinide fullerene compounds will likely lead to the discovery of not only unexpected endohedral fullerene structures, but also to novel actinide clusters, and deepen our understanding of fundamental fullerene chemistry and actinide bonding properties.

4. EXPERIMENTAL DETAILS

Synthesis and Isolation of $U_2C_2@C_{2n}$ ($2n$ = 78, 80). The carbon soot-containing uranium EMFs were produced by the direct-current arc discharge method. The graphite rods, packed with U_3O_8 and graphite powders (molar ratio of U/C = 1:30), were vaporized in the arcing chamber under a 200 Torr helium atmosphere. The resulting soot was collected and refluxed in CS_2 under an argon atmosphere for 12 h. The separation and purification of $U_2C_2@C_{2n}$ ($2n$ = 78, 80) were achieved by multistage HPLC procedures. Multiple HPLC columns, including Buckyprep M (25 × 250 mm, Cosmosil, Nacalai Tesque Inc.), Buckprep-D (10 × 250 mm, Cosmosil, Nacalai Tesque, Japan), Buckprep (10 × 250 mm, Cosmosil, Nacalai Tesque, Japan), Buckprep-M (10 × 250 mm, Cosmosil, Nacalai Tesque, Japan), and 5PBB (10 × 250 mm, Cosmosil, Nacalai Tesque, Japan), were utilized in the procedures. Further details are described in the Supporting Information.

Spectroscopic Studies. The positive-ion mode matrix-assisted laser desorption/ionization time-of-flight (Bruker, Germany) was employed for the mass characterization. The UV−vis−NIR spectra of the purified $U_2C_2@C_{2n}$ ($2n$ = 78, 80) were measured in CS_2 solution with a Cary 5000 UV−vis−NIR spectrophotometer (Agilent, U.S.). The Raman spectra were obtained using a Horiba Lab RAM HR Evolution Raman spectrometer using a laser at 633 nm. The Micro Fourier transform infrared spectra were recorded at room temperature by a Vertex 70 spectrometer (Bruker, Germany) with a resolution of 4 cm^{-1}. For the IR and Raman measurements, the samples were drop-coated on aluminized paper and a quartz plate, respectively. The residual CS_2 was removed in a drying chamber in a vacuum at 40 °C. For the ^{13}C NMR spectroscopic measurements, the $U_2C_2@C_{80}$ sample was dissolved in CS_2 and placed into the NMR tube. A capillary containing acetone-d_6 was used as an internal lock. The ^{13}C NMR spectroscopic measurements were performed at 600 MHz (chemical shift measured in the range from −15 to 250 ppm) with a OneNMR 600 MHz spectrometer (Agilent, U.S.) at 298 and 308 K. X-ray absorption spectroscopy (XAS) experiments were performed at the Shanghai Synchrotron Radiation Facility (SSRF beamline BL14W1).

X-ray Crystallographic Study. The black block crystals of $U_2C_2@C_{2n}$ ($2n$ = 78, 80) were obtained by slow diffusion of a carbon disulfide solution of the corresponding metallofullerene into a benzene solution of [Ni^{II}·(OEP)]. Single-crystal X-ray data of $U_2C_2@C_{80}$ were collected at 100 K using synchrotron radiation (0.82653 Å) with a MX300-HE CCD detector at beamline BL17B of the Shanghai Synchrotron Radiation Facility (SSRF), and X-ray data of $U_2C_2@C_{78}$ were collected at 113 K on a diffractometer (APEX II; Bruker Analytik GmbH) equipped with a CCD collector. The multiscan method was used for absorption correction. The structures were solved using direct methods[48] and refined on F^2 using full-matrix least-squares using the SHELXL2015 crystallographic software package.[49] Hydrogen atoms were inserted at calculated positions and constrained with isotropic thermal parameters.

Crystal data for $U_2C_2@I_h(7)$-C_{80}·[Ni^{II}-(OEP)]·1.5C_6H_6·CS_2: M_r = 2245.63, 0.12 mm × 0.1 mm × 0.1 mm, monoclinic, $P2_1/c$ (No. 14), a = 17.5980(5) Å, b = 16.9502(5) Å, c = 26.7945(7) Å, α = 90°, β =

DOI: 10.1021/jacs.9b10247
J. Am. Chem. Soc. 2019, 141, 20249−20260

106.438(10)°, γ = 90°, V = 7665.8 (4) Å^3, Z = 4, ρ_{calcd} = 1.946 g cm^{-3}, μ(Cu Kα) = 3.182 mm^{-1}, θ = 1.674−30.262, T = 273(2) K, R_1 = 0.0655, wR_2 = 0.1864 for all data; R_1 = 0.0626, wR_2 = 0.1830 for 13 292 reflections ($I > 2.0\sigma(I)$) with 1374 parameters. Goodness-of-fit indicator 1.033. Maximum residual electron density 1.570 e Å^{-3}. CCDC 1953684 contains the crystallographic data.

Crystal data for $U_2C_2@D_{3h}(5)$-C_{78}·[Ni^{II}-(OEP)]·1.5C_6H_6·CS_2: M_r = 2203.76, 0.1 mm × 0.08 mm × 0.06 mm, monoclinic, $P2_1/c$ (No. 14), a = 17.6747(15) Å, b = 16.8738(11) Å, c = 26.3272(15) Å, α = 90°, β = 106.042(7)°, γ = 90°, V = 7546.1(9) Å^3, Z = 4, ρ_{calcd} = 1.940 g cm^{-3}, μ(Cu Kα) = 12.847 mm^{-1}, θ = 3.148−68.500, T = 113(2) K, R_1 = 0.0772, wR_2 = 0.2055 for all data; R_1 = 0.0741, wR_2 = 0.2025 for 12 923 reflections ($I > 2.0\sigma(I)$) with 2058 parameters. Goodness-of-fit indicator 1.031. Maximum residual electron density 2.204 e Å^{-3}. CCDC 1953683 contains the crystallographic data.

Computational Details. Geometry optimizations for $U_2C_2@C_{2n}$ ($2n$ = 78, 80) were performed with Kohn−Sham density functional theory (DFT), using the Amsterdam Density Functional package.[50] The Perdew−Burke−Ernzerhof (PBE)[51,52] and the PBE-based hybrid PBE0[51−53] density functionals were used, in conjunction with all-electron triple-ζ polarized (TZP) Slater-type orbital (STO) basis sets.[54,55] Relativistic effects were included by means of the scalar relativistic (SR) zero-order regular approximation (ZORA).[56] "D3" dispersion corrections[57,58] were included in the calculations. Additional optimizations were carried out with the Gaussian (G16) package,[59] with the PBE and PBE0 functionals, and Gaussian-type orbital (GTO) basis sets as follows: 6-31G(d,p) for C and the SDD basis sets with a matching scalar relativistic effective core potential for U, as provided by the G16 basis set library.[60] IR and Raman spectra were calculated for $U_2C_2@I_h(7)$-C_{80} and $U_2C_2@D_{3h}(5)$-C_{78} with the same GTO basis sets and the PBE0 functional.

Additional DFT and multireference wave function-theory calculations were conducted for a $UC_2U@(C_7H_7)_2$ model complex to shed light on the electronic structure and chemical bonding of the UC_2U motif. In the model system, cycloheptatrienyl ligands represent the interactions of the UC_2U moiety with the C_{80} cage. In a recent study of $U_2C@I_h(7)$-C_{80}, a similar model was shown to represent the interactions between the encapsulated moiety and the cage faithfully.[9] The geometry of $UC_2U@(C_7H_7)_2$ was optimized with SR-ZORA, the PBE0 hybrid functional, all-electron valence triple-ζ doubly polarized (TZ2P) STO basis sets for all atoms, and "D3" augmented with Becke-Johnson damping (D3BJ). The geometry was relaxed fully or by applying constraints, for the ground spin-quintet state, as illustrated in Figure 3. The optimized systems were subjected to natural localized molecular orbital (NLMO) bonding analyses, carried out with NBO6.[61] Further, a structure of $UC_2U@(C_7H_7)_2$ resembling closely the $UC_2U(C_6)_2$ fragment of the $UC_2U@C_{80}$ cluster was created by extracting the $UC_2U(C_6)_2$ motif from the optimized $UC_2U@C_{80}$, replacing the carbon hexagons by cycloheptatrienyl ligands with the same carbon plane orientations, followed by adaption to C_{2v} symmetry (Figure S12, structure **1a**). Multiconfigurational wave functions were then calculated for **1a** in C_{2v} symmetry, within the complete active space self-consistent field (CAS-SCF) framework,[62] using the scalar-relativistic second-order Douglas−Kroll−Hess Hamiltonian[63−66] and ANO-RCC-VTZP basis sets[67−69] for all atoms. The CAS consisted of four electrons distributed among the 10 metal 5f orbitals of nonbonding character with respect to the cycloheptatrienyl ligands (CAS(4,10)). The remaining four 5f metal orbitals have antibonding character with respect to the cycloheptatrienyl ligands and were left inactive as, otherwise, their bonding counterparts with eight electrons needed to be taken as active as well for a balanced description. Such CAS(12,18) computations turned out to be computationally intractable. With CAS(4,10), all resulting spin-states (quintet, triplet, and singlet) were calculated in state-averaged runs for each irreducible representation of C_{2v}. Electronic state energies including the effects from the dynamic electron correlation were attempted with both multiconfigurational on-top pair density functional theory (MC-pDFT), with the fully translated PBE functional,[70] as well as with second-order multireference perturbation theory at second order (PT2). However, MC-pDFT concluded with significant symmetry breaking, whereas the PT2 results suffered from intruder states. We therefore focused on the results from the CAS calculations. Spin orbit coupling (SOC) was treated by restricted active space state interaction (RAS-SI) and atomic mean field integrals (AMFI).[71] All wave function calculations were carried out with a locally modified version of OpenMolcas.[72] Metal−ligand bonding was addressed with NLMO bonding analyses of the ground-state CAS-SO wave function, following the procedure detailed in refs 9 and 73−75.

■ ASSOCIATED CONTENT

Supporting Information

The Supporting Information is available free of charge at https://pubs.acs.org/doi/10.1021/jacs.9b10247.

HPLC profiles for the separation of $U_2C_2@I_h(7)$-C_{80} and $U_2C_2@D_{3h}(5)$-C_{78}; additional single-crystal structural parameters and Raman and IR spectra of $U_2C_2@I_h(7)$-C_{80} and $U_2C_2@D_{3h}(5)$-C_{78}; additional results from computations on $U_2C_2@I_h(7)$-C_{80} and $U_2C_2@D_{3h}(5)$-C_{78} and related systems (relative energies with different functionals, C−C and M−C distances, spin densities, MO diagrams, etc.); and vibrational modes of the Raman spectra of $U_2C_2@C_{80}$ and $U_2C_2@C_{78}$ (PDF)

X-ray crystallographic data for $U_2C_2@I_h(7)$-C_{80} (CIF)

X-ray crystallographic data for $U_2C_2@D_{3h}(5)$-C_{78} (CIF)

■ AUTHOR INFORMATION

Corresponding Authors

*chenning@suda.edu.cn

*jochena@buffalo.edu

ORCID

Laura Abella: 0000-0003-2188-248X

Dumitru-Claudiu Sergentu: 0000-0001-6570-5245

Xiaohong Li: 0000-0003-3190-7214

Shuao Wang: 0000-0002-1526-1102

Luis Echegoyen: 0000-0003-1107-9423

Jochen Autschbach: 0000-0001-9392-877X

Ning Chen: 0000-0002-9405-6229

Author Contributions

⊥J.Z., L.A., and D.-C.S. contributed equally to this work.

Notes

The authors declare no competing financial interest.

■ ACKNOWLEDGMENTS

We cordially thank beamline BL14W1 of the Shanghai Synchrotron Radiation Facility (SSRF) for XAS test and Dr. Cuiying Pei (ShanghaiTech University) for the kind technique support. N.C. thanks the National Science Foundation China (NSFC 51302178), the NSF of Jiangsu Province (BK20171211), the Priority Academic Program Development of Jiangsu Higher Education Institutions (PAPD), and the project of scientific and technologic infrastructure of Suzhou (SZS201708). J.A. acknowledges support from the U.S. Department of Energy, Office of Basic Energy Sciences, Heavy Element Chemistry program, under grant DE-SC0001136, for the calculations on the model systems, and the Center for Actinide Science and Technology (CAST) funded by the Energy Frontiers Research Program under Award Number DE-SC0016568 for the computational studies of the cluster fullerenes. J.A. also thanks the Center for Computational Research (CCR) at the University at Buffalo for providing computational resources. L.E. thanks the U.S.

DOI: 10.1021/jacs.9b10247
J. Am. Chem. Soc. 2019, 141, 20249−20260

National Science Foundation (NSF) for generous support of this work under grant CHE-180317, and the Robert A. Welch Foundation is also gratefully acknowledged for an endowed chair to L.E. (grant AH-0033).

REFERENCES

(1) Guo, T.; Diener, M. D.; Chai, Y.; Alford, M. J.; Haufler, R. E.; McClure, S. M.; Ohno, T.; Weaver, J. H.; Scuseria, G. E.; Smalley, R. E. Uranium Stabilization of C_{28}: A Tetravalent Fullerene. *Science* **1992**, *257*, 1661−1664.

(2) Diener, M. D.; Smith, C. A.; Veirs, D. K. Anaerobic Preparation and Solvent-Free Separation of Uranium Endohedral Metallofullerenes. *Chem. Mater.* **1997**, *9*, 1773−1777.

(3) Akiyama, K.; Zhao, Y.; Sueki, K.; Tsukada, K.; Haba, H.; Nagame, Y.; Kodama, T.; Suzuki, S.; Ohtsuki, T.; Sakaguchi, M.; Kikuchi, K.; Katada, M.; Nakahara, H. Isolation and Characterization of Light Actinide Metallofullerenes. *J. Am. Chem. Soc.* **2001**, *123*, 181−182.

(4) Akiyama, K.; Sueki, K.; Haba, H.; Tsukada, K.; Asai, M.; Yaita, T.; Nagame, Y.; Kikuchi, K.; Katada, M.; Nakahara, H. Production and characterization of actinide metallofullerenes. *J. Radioanal. Nucl. Chem.* **2003**, *255*, 155−158.

(5) Dunk, P. W.; Kaiser, N. K.; Mulet-Gas, M.; Rodriguez-Fortea, A.; Poblet, J. M.; Shinohara, H.; Hendrickson, C. L.; Marshall, A. G.; Kroto, H. W. The smallest stable fullerene, M@C_{28} (M = Ti, Zr, U): stabilization and growth from carbon vapor. *J. Am. Chem. Soc.* **2012**, *134*, 9380−9389.

(6) Wang, Y.; Morales-Martinez, R.; Zhang, X.; Yang, W.; Wang, Y.; Rodriguez-Fortea, A.; Poblet, J. M.; Feng, L.; Wang, S.; Chen, N. Unique Four-Electron Metal-to-Cage Charge Transfer of Th to a C_{82} Fullerene Cage: Complete Structural Characterization of Th@$C_{3v}(8)$-C_{82}. *J. Am. Chem. Soc.* **2017**, *139*, 5110−5116.

(7) Cai, W.; Morales-Martinez, R.; Zhang, X.; Najera, D.; Romero, E. L.; Metta-Magana, A.; Rodriguez-Fortea, A.; Fortier, S.; Chen, N.; Poblet, J. M.; Echegoyen, L. Single crystal structures and theoretical calculations of uranium endohedral metallofullerenes (U@C_{2n}, $2n$ = 74, 82) show cage isomer dependent oxidation states for U. *Chem. Sci.* **2017**, *8*, 5282−5290.

(8) Zhang, X.; Wang, Y.; Morales-Martinez, R.; Zhong, J.; de Graaf, C.; Rodriguez-Fortea, A.; Poblet, J. M.; Echegoyen, L.; Feng, L.; Chen, N. U_2@$I_h(7)$-C_{80}: Crystallographic Characterization of a Long-Sought Dimetallic Actinide Endohedral Fullerene. *J. Am. Chem. Soc.* **2018**, *140*, 3907−3915.

(9) Zhang, X.; Li, W.; Feng, L.; Chen, X.; Hansen, A.; Grimme, S.; Fortier, S.; Sergentu, D. C.; Duignan, T. J.; Autschbach, J.; Wang, S.; Wang, Y.; Velkos, G.; Popov, A. A.; Aghdassi, N.; Duhm, S.; Li, X.; Li, J.; Echegoyen, L.; Schwarz, W. H. E.; Chen, N. A diuranium carbide cluster stabilized inside a C_{80} fullerene cage. *Nat. Commun.* **2018**, *9*, 2753−2760.

(10) Cai, W.; Abella, L.; Zhuang, J.; Zhang, X.; Feng, L.; Wang, Y.; Morales-Martinez, R.; Esper, R.; Boero, M.; Metta-Magana, A.; Rodriguez-Fortea, A.; Poblet, J. M.; Echegoyen, L.; Chen, N. Synthesis and Characterization of Non-Isolated-Pentagon-Rule Actinide Endohedral Metallofullerenes U@$C_1(17418)$-C_{76}, U@$C_1(28324)$-C_{80}, and Th@$C_1(28324)$-C_{80}: Low-Symmetry Cage Selection Directed by a Tetravalent Ion. *J. Am. Chem. Soc.* **2018**, *140*, 18039−18050.

(11) Cai, W.; Chen, C. H.; Chen, N.; Echegoyen, L. Fullerenes as Nanocontainers That Stabilize Unique Actinide Species Inside: Structures, Formation, and Reactivity. *Acc. Chem. Res.* **2019**, *52*, 1824−1833.

(12) Wang, Y.; Morales-Martinez, R.; Cai, W.; Zhuang, J.; Yang, W.; Echegoyen, L.; Poblet, J. M.; Rodriguez-Fortea, A.; Chen, N. Th@$C_1(11)$-C_{86}: an actinide encapsulated in an unexpected C_{86} fullerene cage. *Chem. Commun.* **2019**, *55*, 9271−9274.

(13) Hachiya, M.; Nikawa, H.; Mizorogi, N.; Tsuchiya, T.; Lu, X.; Akasaka, T. Exceptional chemical properties of Sc@$C_{2v}(9)$-C_{82} probed with adamantylidene carbene. *J. Am. Chem. Soc.* **2012**, *134*, 15550−15555.

(14) Sato, S.; Nikawa, H.; Seki, S.; Wang, L.; Luo, G.; Lu, J.; Haranaka, M.; Tsuchiya, T.; Nagase, S.; Akasaka, T. A co-crystal composed of the paramagnetic endohedral metallofullerene La@C_{82} and a nickel porphyrin with high electron mobility. *Angew. Chem., Int. Ed.* **2012**, *51*, 1589−1591.

(15) Suzuki, M.; Lu, X.; Sato, S.; Nikawa, H.; Mizorogi, N.; Slanina, Z.; Tsuchiya, T.; Nagase, S.; Akasaka, T. Where does the metal cation stay in Gd@$C_{2v}(9)$-C_{82}? A single-crystal X-ray diffraction study. *Inorg. Chem.* **2012**, *51*, 5270−5273.

(16) Wang, X.; Andrews, L.; Malmqvist, P.-Å.; Roos, B. O.; Gonçalves, A. P.; Pereira, C. C. L.; Marçalo, J.; Godart, C.; Villeroy, B. Infrared Spectra and Quantum Chemical Calculations of the Uranium Carbide Molecules UC and CUC with Triple Bonds. *J. Am. Chem. Soc.* **2010**, *132*, 8484−8488.

(17) Utton, C. A.; De Bruycker, F.; Boboridis, K.; Jardin, R.; Noel, H.; Guéneau, C.; Manara, D. Laser melting of uranium carbides. *J. Nucl. Mater.* **2009**, *385*, 443−448.

(18) Gupta, S. K.; Gingerich, K. A. Observation and atomization energies of the gaseous uranium carbides, UC, UC_2, UC_3, UC_4, UC_5, and UC_6 by high temperature mass spectrometry. *J. Chem. Phys.* **1979**, *71*, 3072−3080.

(19) Mankad, V. H.; Jha, P. K. Thermodynamic properties of nuclear material uranium carbide using density functional theory. *J. Therm. Anal. Calorim.* **2016**, *124*, 11−20.

(20) Du, J.; Jiang, G. A Systematic Theoretical Study of UC_6: Structure, Bonding Nature, and Spectroscopy. *Inorg. Chem.* **2017**, *56*, 13794−13800.

(21) Olmstead, M. M.; Costa, D. A.; Maitra, K.; Noll, B. C.; Phillips, S. L.; Van Calcar, P. M.; Balch, A. L. Interaction of Curved and Flat Molecular Surfaces. The Structures of Crystalline Compounds Composed of Fullerene (C_{60}, $C_{60}O$, C_{70}, and $C_{120}O$) and Metal Octaethylporphyrin Units. *J. Am. Chem. Soc.* **1999**, *121*, 7090−7097.

(22) Tashiro, K.; Aida, T. Metalloporphyrin hosts for supramolecular chemistry of fullerenes. *Chem. Soc. Rev.* **2007**, *36*, 189−197.

(23) Popov, A. A.; Yang, S.; Dunsch, L. Endohedral fullerenes. *Chem. Rev.* **2013**, *113*, 5989−6113.

(24) Kurihara, H.; Lu, X.; Iiduka, Y.; Nikawa, H.; Hachiya, M.; Mizorogi, N.; Slanina, Z.; Tsuchiya, T.; Nagase, S.; Akasaka, T. X-ray structures of Sc_2C_2@C_{2n} (n = 40−42): in-depth understanding of the core-shell interplay in carbide cluster metallofullerenes. *Inorg. Chem.* **2012**, *51*, 746−750.

(25) Sado, Y.; Aoyagi, S.; Izumi, N.; Kitaura, R.; Kowalczyk, T.; Wang, J.; Irle, S.; Nishibori, E.; Sugimoto, K.; Shinohara, H. Structure of Tm_2 and Tm_2C_2 encapsulated in low-symmetry $C_{82}(C_s(6))$ fullerene cage by single crystal X-ray diffraction. *Chem. Phys. Lett.* **2014**, *600*, 38−42.

(26) Liu, F.; Wei, T.; Wang, S.; Guan, J.; Lu, X.; Yang, S. A Bent Tb_2C_2Cluster Encaged in a $C_s(6)$-C_{82}Cage: Synthesis, Isolation and X-ray Crystallographic Study. *Fullerenes, Nanotubes, Carbon Nanostruct.* **2014**, *22*, 215−226.

(27) Chen, C. H.; Ghiassi, K. B.; Ceron, M. R.; Guerrero-Ayala, M. A.; Echegoyen, L.; Olmstead, M. M.; Balch, A. L. Beyond the Butterfly: Sc_2C_2@$C_{2v}(9)$-C_{86}, an Endohedral Fullerene Containing a Planar, Twisted Sc_2C_2 Unit with Remarkable Crystalline Order in an Unprecedented Carbon Cage. *J. Am. Chem. Soc.* **2015**, *137*, 10116−10119.

(28) Chen, C. H.; Abella, L.; Ceron, M. R.; Guerrero-Ayala, M. A.; Rodriguez-Fortea, A.; Olmstead, M. M.; Powers, X. B.; Balch, A. L.; Poblet, J. M.; Echegoyen, L. Zigzag Sc_2C_2 Carbide Cluster inside a [88]Fullerene Cage with One Heptagon, Sc_2C_2@C_s(hept)-C_{88}: A Kinetically Trapped Fullerene Formed by C2 Insertion? *J. Am. Chem. Soc.* **2016**, *138*, 13030−13037.

(29) Wang, Y.; Tang, Q.; Feng, L.; Chen, N. Sc_2C_2@D_{3h}(14246)-C_{74}: A Missing Piece of the Clusterfullerene Puzzle. *Inorg. Chem.* **2017**, *56*, 1974−1980.

(30) Falcone, M.; Barluzzi, L.; Andrez, J.; Fadaei Tirani, F.; Zivkovic, I.; Fabrizio, A.; Corminboeuf, C.; Severin, K.; Mazzanti, M. The role

DOI: 10.1021/jacs.9b10247
J. Am. Chem. Soc. 2019, 141, 20249−20260

of bridging ligands in dinitrogen reduction and functionalization by uranium multimetallic complexes. *Nat. Chem.* **2019**, *11*, 154−160.
(31) Falcone, M.; Scopelliti, R.; Mazzanti, M. CO_2 and CO/H_2 Conversion to Methoxide by a Uranium(IV) Hydride. *J. Am. Chem. Soc.* **2019**, *141*, 9570−9577.
(32) Cantat, T.; Arliguie, T.; Noël, A.; Thuéry, P.; Ephritikhine, M.; Floch, P. L.; Mézailles, N. The U═C Double Bond: Synthesis and Study of Uranium Nucleophilic Carbene Complexes. *J. Am. Chem. Soc.* **2009**, *131*, 963−972.
(33) Tourneux, J.-C.; Berthet, J.-C.; Cantat, T.; Thuéry, P.; Mézailles, N.; Le Floch, P.; Ephritikhine, M. Uranium(IV) Nucleophilic Carbene Complexes. *Organometallics* **2011**, *30*, 2957−2971.
(34) Evans, W. J.; Siladke, N. A.; Ziller, J. W. Synthesis and Reactivity of a Silylalkyl Double Tuck-in Uranium Metallocene $[(\eta_5{:}\eta_1\text{-}C_5Me_4SiMe_2CH_2)_2U]$ and its Conversion to Bis(tethered) Metallocenes. *Chem. - Eur. J.* **2010**, *16*, 796−800.
(35) Korobkov, I.; Gorelsky, S.; Gambarotta, S. Reduced Uranium Complexes: Synthetic and DFT Study of the Role of π Ligation in the Stabilization of Uranium Species in a Formal Low-Valent State. *J. Am. Chem. Soc.* **2009**, *131*, 10406−10420.
(36) Tourneux, J. C.; Berthet, J. C.; Cantat, T.; Thuery, P.; Mezailles, N.; Ephritikhine, M. Exploring the uranyl organometallic chemistry: from single to double uranium-carbon bonds. *J. Am. Chem. Soc.* **2011**, *133*, 6162−6165.
(37) Ma, G.; Ferguson, M. J.; McDonald, R.; Cavell, R. G. Actinide metals with multiple bonds to carbon: synthesis, characterization, and reactivity of U(IV) and Th(IV) bis(iminophosphorano)methandiide pincer carbene complexes. *Inorg. Chem.* **2011**, *50*, 6500−6508.
(38) Su, W.; Pan, S.; Sun, X.; Wang, S.; Zhao, L.; Frenking, G.; Zhu, C. Double dative bond between divalent carbon(0) and uranium. *Nat. Commun.* **2018**, *9*, 4997.
(39) Cai, W.; Bao, L.; Zhao, S.; Xie, Y.; Akasaka, T.; Lu, X. Anomalous Compression of $D_5(450)$-C_{100} by Encapsulating La_2C_2 Cluster instead of La_2. *J. Am. Chem. Soc.* **2015**, *137*, 10292−10296.
(40) Cai, W.; Li, F. F.; Bao, L.; Xie, Y.; Lu, X. Isolation and Crystallographic Characterization of $La_2C_2@C_s(574)$-C_{102} and $La_2C_2@C_2(816)$-C_{104}: Evidence for the Top-Down Formation Mechanism of Fullerenes. *J. Am. Chem. Soc.* **2016**, *138*, 6670−6675.
(41) Zhao, S.; Zhao, P.; Cai, W.; Bao, L.; Chen, M.; Xie, Y.; Zhao, X.; Lu, X. Stabilization of Giant Fullerenes $C_2(41)$-C_{90}, $D_3(85)$-C_{92}, $C_1(132)$-C_{94}, $C_2(157)$-C_{96}, and $C_1(175)$-C_{98} by Encapsulation of a Large La_2C_2 Cluster: The Importance of Cluster-Cage Matching. *J. Am. Chem. Soc.* **2017**, *139*, 4724−4728.
(42) Pan, C.; Shen, W.; Yang, L.; Bao, L.; Wei, Z.; Jin, P.; Fang, H.; Xie, Y.; Akasaka, T.; Lu, X. Crystallographic characterization of Y_2C_{2n} ($2n$ = 82, 88−94): direct Y−Y bonding and cage-dependent cluster evolution. *Chem. Sci.* **2019**, *10*, 4707−4713.
(43) Olmstead, M. M.; de Bettencourt-Dias, A.; Duchamp, J. C.; Stevenson, S.; Marciu, D.; Dorn, H. C.; Balch, A. L. Isolation and Structural Characterization of the Endohedral Fullerene $Sc_3N@C_{78}$. *Angew. Chem., Int. Ed.* **2001**, *40*, 1223−1225.
(44) Li, F.-F.; Chen, N.; Mulet-Gas, M.; Triana, V.; Murillo, J.; Rodríguez-Fortea, A.; Poblet, J. M.; Echegoyen, L. $Ti_2S@D_{3h}(24109)$-C_{78}: a sulfide cluster metallofullerene containing only transition metals inside the cage. *Chem. Sci.* **2013**, *4*, 3404.
(45) Stevenson, S.; Rice, G.; Glass, T.; Harich, K.; Cromer, F.; Jordan, M. R.; Craft, J.; Hadju, E.; Bible, R.; Olmstead, M. M.; Maitra, K.; Fisher, A. J.; Balch, A. L.; Dorn, H. C. Small-bandgap endohedral metallofullerenes in high yield and purity. *Nature* **1999**, *401*, 55−57.
(46) Yamada, M.; Someya, C.; Wakahara, T.; Tsuchiya, T.; Maeda, Y.; Akasaka, T.; Yoza, K.; Horn, E.; Liu, M. T. H.; Mizorogi, N.; Nagase, S. Metal Atoms Collinear with the Spiro Carbon of 6,6-Open Adducts, $M_2@C_{80}$(Ad) (M = La and Ce, Ad = Adamantylidene). *J. Am. Chem. Soc.* **2008**, *130*, 1171−1176.
(47) Yamada, M.; Mizorogi, N.; Tsuchiya, T.; Akasaka, T.; Nagase, S. Synthesis and Characterization of the D_{5h} Isomer of the Endohedral Dimetallofullerene $Ce_2@C_{80}$: Two-Dimensional Circulation of Encapsulated Metal Atoms Inside a Fullerene Cage. *Chem. - Eur. J.* **2009**, *15*, 9486−9493.
(48) Dolomanov, O. V.; Bourhis, L. J.; Gildea, R. J.; Howard, J. A. K.; Puschmann, H. OLEX2: a complete structure solution, refinement and analysis program. *J. Appl. Crystallogr.* **2009**, *42*, 339−341.
(49) Sheldrick, G. Crystal structure refinement with SHELXL. *Acta Crystallogr., Sect. C: Struct. Chem.* **2015**, *71*, 3−8.
(50) Baerends, E. J.; Ziegler, T.; Atkins, A.; Autschbach, J.; Bashford, D.; Baseggio, O.; Bérces, A.; Bickelhaupt, F.; Bo, C.; Boerritger, P. *ADF2017; SCM, Theoretical Chemistry*; Vrije Universiteit: Amsterdam, The Netherlands, 2017.
(51) Perdew, J. P.; Burke, K.; Ernzerhof, M. Generalized Gradient Approximation Made Simple. *Phys. Rev. Lett.* **1996**, *77*, 3865−3868.
(52) Perdew, J. P.; Burke, K.; Ernzerhof, M. Generalized Gradient Approximation Made Simple. *Phys. Rev. Lett.* **1997**, *78*, 1396−1396.
(53) Adamo, C.; Barone, V. Toward reliable density functional methods without adjustable parameters: The PBE0 model. *J. Chem. Phys.* **1999**, *110*, 6158−6170.
(54) Becke, A. D. Density functional calculations of molecular bond energies. *J. Chem. Phys.* **1986**, *84*, 4524−4529.
(55) Perdew, J. P. Density-functional approximation for the correlation energy of the inhomogeneous electron gas. *Phys. Rev. B: Condens. Matter Mater. Phys.* **1986**, *33*, 8822−8824.
(56) Lenthe, E. v.; Baerends, E. J.; Snijders, J. G. Relativistic regular two-component Hamiltonians. *J. Chem. Phys.* **1993**, *99*, 4597−4610.
(57) Grimme, S.; Antony, J.; Ehrlich, S.; Krieg, H. A consistent and accurate ab initio parametrization of density functional dispersion correction (DFT-D) for the 94 elements H-Pu. *J. Chem. Phys.* **2010**, *132*, 154104.
(58) Grimme, S.; Ehrlich, S.; Goerigk, L. Effect of the damping function in dispersion corrected density functional theory. *J. Comput. Chem.* **2011**, *32*, 1456−1465.
(59) Frisch, M.; Trucks, G.; Schlegel, H.; Scuseria, G.; Robb, M.; Cheeseman, J.; Scalmani, G.; Barone, V.; Petersson, G.; Nakatsuji, H. *Gaussian 16*, revision B.01; Gaussian, Inc.: Wallingford, CT, 2016.
(60) Cao, X.; Dolg, M. Segmented contraction scheme for small-core lanthanide pseudopotential basis sets. *J. Mol. Struct.: THEOCHEM* **2002**, *581*, 139−147.
(61) Glendening, E. D.; Landis, C. R.; Weinhold, F. NBO 6.0: natural bond orbital analysis program. *J. Comput. Chem.* **2013**, *34*, 1429−1437.
(62) Roos, B. O.; Taylor, P. R.; Siegbahn, P. E. M. A complete active space SCF method (CASSCF) using a density matrix formulated super-CI approach. *Chem. Phys.* **1980**, *48*, 157−173.
(63) Douglas, M.; Kroll, N. M. Quantum electrodynamical corrections to the fine structure of helium. *Ann. Phys.* **1974**, *82*, 89−155.
(64) Hess, B. A. Applicability of the no-pair equation with free-particle projection operators to atomic and molecular structure calculations. *Phys. Rev. A: At., Mol., Opt. Phys.* **1985**, *32*, 756−763.
(65) Hess, B. A. Relativistic electronic-structure calculations employing a two-component no-pair formalism with external-field projection operators. *Phys. Rev. A: At., Mol., Opt. Phys.* **1986**, *33*, 3742−3748.
(66) Wolf, A.; Reiher, M.; Hess, B. A. The generalized Douglas−Kroll transformation. *J. Chem. Phys.* **2002**, *117*, 9215−9226.
(67) Widmark, P.-O.; Malmqvist, P.-Å.; Roos, B. O. Density matrix averaged atomic natural orbital (ANO) basis sets for correlated molecular wave functions. *Theor. Chim. Acta.* **1990**, *77*, 291−306.
(68) Roos, B. O.; Lindh, R.; Malmqvist, P.-Å.; Veryazov, V.; Widmark, P.-O. New relativistic ANO basis sets for actinide atoms. *Chem. Phys. Lett.* **2005**, *409*, 295−299.
(69) Roos, B. O.; Lindh, R.; Malmqvist, P.-Å.; Veryazov, V.; Widmark, P.-O. Main group atoms and dimers studied with a new relativistic ANO basis set. *J. Phys. Chem. A* **2004**, *108*, 2851−2858.
(70) Gagliardi, L.; Truhlar, D. G.; Li Manni, G.; Carlson, R. K.; Hoyer, C. E.; Bao, J. L. Multiconfiguration Pair-Density Functional Theory: A New Way To Treat Strongly Correlated Systems. *Acc. Chem. Res.* **2017**, *50*, 66−73.

DOI: 10.1021/jacs.9b10247
J. Am. Chem. Soc. 2019, 141, 20249−20260

(71) Malmqvist, P. Å.; Roos, B. O.; Schimmelpfennig, B. The restricted active space (RAS) state interaction approach with spin−orbit coupling. *Chem. Phys. Lett.* **2002**, *357*, 230−240.
(72) Aquilante, F.; Autschbach, J.; Carlson, R. K.; Chibotaru, L. F.; Delcey, M. G.; De Vico, L.; Fdez. Galván, I.; Ferré, N.; Frutos, L. M.; Gagliardi, L.; Garavelli, M.; Giussani, A.; Hoyer, C. E.; Li Manni, G.; Lischka, H.; Ma, D.; Malmqvist, P. Å.; Müller, T.; Nenov, A.; Olivucci, M.; Pedersen, T. B.; Peng, D.; Plasser, F.; Pritchard, B.; Reiher, M.; Rivalta, I.; Schapiro, I.; Segarra-Martí, J.; Stenrup, M.; Truhlar, D. G.; Ungur, L.; Valentini, A.; Vancoillie, S.; Veryazov, V.; Vysotskiy, V. P.; Weingart, O.; Zapata, F.; Lindh, R. Molcas 8: New capabilities for multiconfigurational quantum chemical calculations across the periodic table. *J. Comput. Chem.* **2016**, *37*, 506−541.
(73) Sergentu, D. C.; Duignan, T. J.; Autschbach, J. Ab Initio Study of Covalency in the Ground versus Core-Excited States and X-ray Absorption Spectra of Actinide Complexes. *J. Phys. Chem. Lett.* **2018**, *9*, 5583−5591.
(74) Autschbach, J. Orbitals for Analyzing Bonding and Magnetism of Heavy-Metal Complexes. *Comments Inorg. Chem.* **2016**, *36*, 215−244.
(75) Gendron, F.; Paez-Hernandez, D.; Notter, F. P.; Pritchard, B.; Bolvin, H.; Autschbach, J. Magnetic properties and electronic structure of neptunyl(VI) complexes: wavefunctions, orbitals, and crystal-field models. *Chem. - Eur. J.* **2014**, *20*, 7994−8011.

DOI: 10.1021/jacs.9b10247
J. Am. Chem. Soc. 2019, 141, 20249−20260